Minimal Models to Capture the Dynamics of a Rotary Unmanned Aerial Vehicle

Rejina Ling Wei Choi[2], Christopher E Hann[1], and XiaoQi Chen[2]

[1]*Department of Electrical and Computer Engineering, University of Canterbury, Christchurch, New Zealand.*
[2]*Department of Mechanical Engineering, University of Canterbury, Christchurch, New Zealand.*

Email: rejina.choi@pg.canterbury.ac.nz

Abstract

This paper presents a method for characterising the primary dynamics of a rotary unmanned aerial vehicle. Based on first principles and basic aerodynamics, a mathematical model which explains the rigid body dynamics of a model-scale helicopter is developed. This model is reduced to three simplified decoupled models of attitude dynamics. Empirical test data is collected from a field experiment with significant wind disturbances. The method worked accurately on both uncoupled and fully coupled attitude models. An integral based parameter identification method is presented to identify the unknown intrinsic helicopter parameters as well as model of wind disturbance. An extended Kalman filter system identification method and common nonlinear regression are used for comparison. The EKF was found to be highly dependent on the initial states, so is not suitable for this application which contains significant disturbance and modelling errors. Nonlinear regression proved to be sufficiently accurate but computationally expensive. The proposed integral based parameter identification method was shown to be fast and accurate and is well suited to this application.

Keywords: *Unmanned Aerial Vehicle, minimal modelling, integral-based parameter identification, Extended Kalman Filter, disturbance*

1 INTRODUCTION

There has been significant research interest in designing small-scale helicopters, mainly due to their agility and maneuverability. By directing the thrust force of the main rotor accordingly, helicopters are capable of vertical flight as well as translational movement. Thus, helicopters have an advantage over fixed wing aircraft as they do not need translational velocity to produce aerodynamic flight forces. However, the complicated nonlinear dynamics of a scaled-model helicopter make the modelling and control design a challenging task.

Early research on the identification scheme and control design for a model-scaled helicopter are based on linearized dynamics [1] of the helicopter using the concept of stability derivatives. Flight dynamics modelling are typically broken into operating regions such as hovering or forward flight. The model is valid within a certain frequency range, where good linear correlation between angular rate and cyclic inputs is found [2]. A few papers [3-5] directly identified the nonlinear model dynamics using state-space identification method and EKF. However, they often require good initial estimates of states which may not always be available.

First principles modelling typically produces a nonlinear dynamic model and an extended flight envelope, which provides the capability of extracting linear models at various trim operating points [6]. The main drawback of this approach is that extensive knowledge of helicopter dynamics is required. Furthermore significant experimentation and tuning is needed to accurately determine the underlying physical parameters. System identification [7] can be combined with first principles modeling to identify the unknown or uncertain physical parameters. Typical approaches of system identification in time-domain are the prediction error method (PEM)[8], maximum likelihood method [9], equation

error method and output error method [10]. However, these method are usually very time consuming, sensitive to starting point and with no guarantee of global optimality [11].

In this paper, a simplified model for pitch, roll and yaw dynamics is derived from a complex nonlinear model. It was found that a fully decoupled model in pitch, roll and yaw was able to capture data equally well compared to a more complex model with state coupling. Even though the complex model is theoretically more accurate, the significant wind disturbance and other unknown dynamics dominate. Thus, the simplified model is much more suitable given significantly less computational requirements and its ease of analysis. In addition, a major advantage of a simpler model is the potential for real time implementation, which is a key motivation for the methods developed in this paper.

Specifically, changing wind conditions will change the angle of attack and thus the centre of pressure of actuation surfaces. Hence important parameters like torque constants and damping associated with the attitude dynamics will change over time. There may also be unmodelled flow disturbances that significantly change the helicopter dynamics compared to a calm day or indoor environment. Therefore this paper is focussed on robust minimal modelling methods in difficult environments to ensure the methods developed are extendable to all types of atmospheric conditions during flight.

An integral based parameter identification method [12-14] which was published in the biomedical field is significantly extended to account for disturbance and modeling error. Specifically, the methods published in the biomedical field are for open loop diagnosis with a low sampling rate and are not designed for control applications where the sampling rate is very high and there

are significant disturbances. In addition, the accuracy of this method is compared to the Extended Kalman Filter (EKF), which is another fast parameter identification method that is potentially comparable to the integral method. However, this comparison has not yet been performed in the literature. The integral method is also compared against standard non-linear regression to test the computational efficiency and accuracy.

The paper is organized as follows: In Section 2, the experimental set up and data acquisition are described. In Section 3, the model-scaled helicopter attitude dynamics model structure is presented. Section 4 describes the integral-based parameter identification method and Section 5 shows the Extended Kalman Filter parameter estimation method. In Section 6 the identification results obtained from the two methods are compared and in Section 7 the conclusions and future work are given.

2 METHODOLOGY

2.1 Experimental setup and data acquisition

Obtaining open loop responses to characterize a helicopter flying in an outdoor environment is not feasible. Hence a number of manoeuvres were executed by a test pilot via a remote control system. In the experiment, a varying frequency sweep input signal was used to provide data for system identification, which includes potential coupling in the inputs and outputs. The helicopter was initially piloted to slowly take off to a certain height, then a sinusoidal low frequency excitation signal of approximately 1~3Hz was applied on one of the cyclic inputs before hover at trim position again. As the helicopter take-off dynamics are not considered in the model, the flight data is truncated and

collected from the point where the hovering stage begins. Therefore, the helicopter was essentially performing lateral and longitudinal flight motion. The input-output data was recorded at a sampling rate of 100Hz and passed through a low pass filter which has cut-off frequency at 15Hz to remove undesired information such as structural vibrations. It is recommended that the filter for all the output and input is chosen with a cut-off frequency 5 times higher than the maximum frequency of the excitation signal [7].

In order to record the data for identification, data logging is implemented through an onboard Mobisense MBS270 embedded computer. MBS270 runs as a standalone computer with kernel and file system in flash that support Linux OS. Thus, it offers faster software development since the program can be developed in the high-level programming language in C/C++ with supplied open source libraries. The Mobisense MBS270 is the central processing unit in our application which interfaces with an Inertial Measurement Unit (IMU) from MicroStrain 3DGX1 via RS232 serial interface to log the helicopter attitude information. The IMU unit performs the filtering and processing on the raw sensory output data from accelerometer, gyroscopes, and magnetometers to output linear acceleration, angular rates and orientation of the helicopter.

A separate microcontroller Arduino Duemilanove is also used for reading the helicopter actuation input which are the pulse width signal for four servo motors. The four servo motors are the actuation input to the helicopter. Three of them are arranged in 120 degrees around swash plate so that each servo motor can elevate one side of swash plate and their combined efforts enable cyclic and collective pitch on main rotors blade. The last servo motor is for applying pedal input to the helicopter by adjusting the tail rotor blade pitch angle. The recorded servo signals are then transferred to the MBS270 through UART line.

The input output data collected during flight test is stored into a microSD memory card on MBS270 as a text file and then transferred to a PC workstation for analysis after landing. The overall architecture of the data acquisition system is shown in Fig. 1.

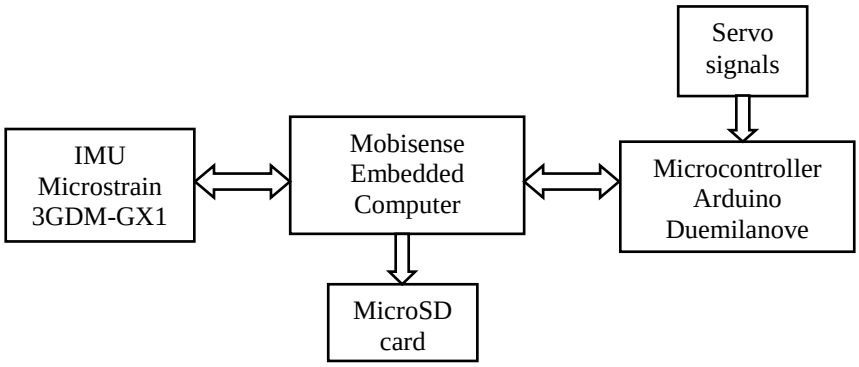

Fig. 1 Architecture of Data Acquisition System

The Trex 600 ESP remote control (RC) helicopter is a model helicopter chosen as the platform for carrying out the data measurement on real flight due to its sufficient payload capacity, great manoeuvrability and low cost replacement parts. It is equipped with Bell-Hiller stabilizer bar and has a two-bladed rotor of 0.6m radius. The dry weight is 3.3kg and allows payload of 2kg with operation time of about 15 minutes. Trex 600 with the necessary instrumentation equipment installed is shown in Fig. 2.

Fig. 2 Modified Trex600 with instrumentation equipment installed

2.2 Modelling structure

For modelling a model-scale helicopter, a standard six degree of freedom (DOF) model is used. The axes of rotation of the helicopter are shown in Fig. 3. The standard equation describing angular velocity in the body frame is defined:

$$\dot{\boldsymbol{\omega}}^B = \mathbf{I}^{-1}(\mathbf{I}\boldsymbol{\omega}^B \times \boldsymbol{\omega}^B) + \mathbf{I}^{-1}\boldsymbol{\tau}^B \tag{1}$$

$$\boldsymbol{\omega}^B = [p \quad q \quad r]^T \tag{2}$$

$$\boldsymbol{\tau}^B = [M_\phi \quad M_\theta \quad M_\psi] \tag{3}$$

$$\mathbf{I} = \begin{pmatrix} I_{xx} & 0 & -I_{xz} \\ 0 & I_{yy} & 0 \\ -I_{xz} & 0 & I_{zz} \end{pmatrix} \tag{4}$$

where $\boldsymbol{\omega}^B$ is the angular velocity in body fixed reference frame, $\boldsymbol{\tau}^B$ is the moment components along body axes, and $\mathbf{I}$ is the fuselage inertial matrix in body coordinates. Due to the symmetry of the helicopter with respect to the $x_B - z_B$ plane, the terms I_{xy} and I_{yz} are zero. Although I_{xz} is non-zero, but the value is typically much smaller than the other terms, thus it will be ignored in the model.

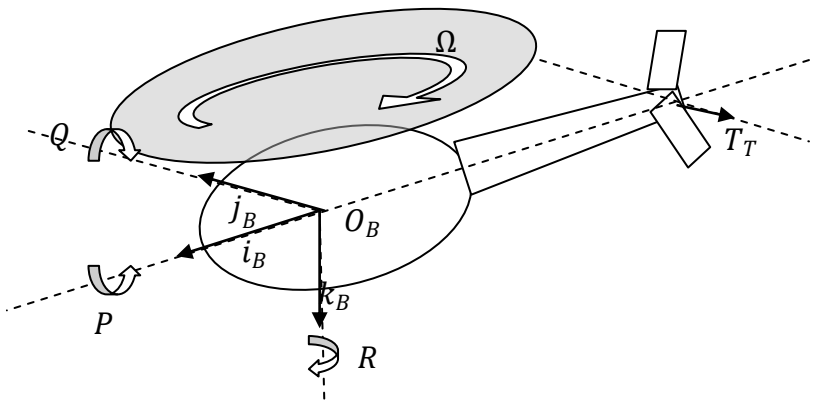

Fig. 3 Six degree of freedom of helicopter in body frame

After some analytical manipulation, Equation (1) can be broken down into:

$$\begin{aligned}\dot{p} &= \frac{(I_{yy} - I_{zz})}{I_{xx}} qr + \frac{1}{I_{xx}} M_{\phi} \\ \dot{q} &= \frac{(I_{zz} - I_{xx})}{I_{yy}} pr + \frac{1}{I_{yy}} M_{\theta} \\ \dot{r} &= \frac{(I_{xx} - I_{yy})}{I_{zz}} pq + \frac{1}{I_{zz}} M_{\psi}\end{aligned} \tag{5}$$

where p, q, r are the helicopter's roll rate, pitch rate and yaw rate respectively, and $M_{\phi}, M_{\theta}, M_{\psi}$ are the roll moment, pitch moment and yaw moment respectively.

The external moment acting on the helicopter rigid body are mainly contributed by the main rotor. By varying the angle of attack of the main rotor blade or cyclic pitch angle, an aerodynamic lift force is created. The pitch and roll moment of the helicopter are generated through the difference in the lift force in lateral and longitudinal axes. The equations for the moment M_{ϕ} and M_{θ} in Equation (5) are defined:

$$\begin{bmatrix} M_{\phi} \\ M_{\theta} \end{bmatrix} = \frac{n}{2\pi} \int_0^{2\pi} \int_0^{BR} l \begin{bmatrix} \sin(\zeta + \frac{\pi}{2}) \\ -\cos(\zeta + \frac{\pi}{2}) \end{bmatrix} dL_m d\xi \tag{6}$$

$$dL_m = \frac{1}{2} \rho (\Omega l)^2 ac [\alpha_3 (\frac{L_3}{L_1(L_2 + L_3)} \delta_{cyc} + \frac{L_2 L_4}{L_1(L_2 + L_3)} \beta) - \alpha_4 \frac{\omega_{M2}}{\Omega}] \tag{7}$$

where α_3, α_4 is a correction factor to compensate for simplified aerodynamics, $L_{1,2,3,4,}$ are the linkage lengths in rotor hub assembly, ρ is the air density, Ω is the main rotor angular velocity, l is the position along the main rotor blade, and a is the main rotor lift slope, c is the main blade chord length and dL_m is the main rotor aerodynamics lift element. Equation (6) indicates that the pitch and roll

moments depend on the pitch and roll input command through δ_{cyc} as well as on the flybar flapping angle β. The last term in Equation (7) is due to the gyroscopic effect of the rotating blade, which is the ratio between the second element of the angular velocity vector of main rotor blade ω_{M2} and main rotor rotational speed [15].

For a full-scale helicopter, the stability is achieved by having bigger body size and also the flapping mechanism on the rotor hub. Flapping dynamics are commonly modelled in the literature [16,17]. However, RC helicopters have a hingeless rotor hub and are equipped with a flybar to increase damping on lateral and longitudinal flight motion, and enhance the stability of the helicopter. Therefore, this paper specifically chose the flybar dynamics instead of flapping dynamics as the base model for demonstrating that the simplified models can perform equally well to complex model in the presence of disturbances during flight. Preliminary investigation showed that since the thrust vector is normal to the main rotor plane, whenever a flapping angle is present, the cyclic collective input generates a moment on helicopter attitude dynamics. Therefore, a cyclic collective term is investigated to see if it improves prediction of attitude dynamics as compared to simpler models that lump this effect into other parameters.

The Flybar flapping angle derivation starts from defining dynamics of flybar in the Euler equation [18]:

$$\boldsymbol{\tau}_F = \boldsymbol{\omega}_F \times \mathbf{I}_F \boldsymbol{\omega}_F + \mathbf{I}_F \dot{\boldsymbol{\omega}}_F \tag{8}$$

$$\begin{bmatrix} \tau_{F1} \\ n\int_{R_1}^{BR_2} r dL \\ \tau_{F3} \end{bmatrix} = \begin{bmatrix} 0 \\ -I_f \omega_{F1} \omega_{F3} \\ I_f \omega_{F1} \omega_{F2} \end{bmatrix} + \begin{bmatrix} 0 \\ I_f \dot{\omega}_{F2} \\ I_f \dot{\omega}_{F3} \end{bmatrix} \tag{9}$$

where I_f is the unified rotational inertial of the flybar. The parameters $\tau_{F1,}\tau_{F2},\tau_{F3}$ are the external moment applied to flybar, which can be obtained by integrated lift elements dL along the length of flybar and $\omega_{F1},\omega_{F2},\omega_{F3}$ are the angular velocities of flybar around i_B, j_B and k_B axes in Fig. 3.

After defining the flybar angular velocity, inertial and external forces, the flybar flapping angle is defined [18] :

$$\beta = \beta_o \left(\frac{\alpha_1 L_7 L_8}{L_5 L_6 L_9} (-\delta_\theta \cos\xi - \delta_\phi \sin\xi) + \frac{\alpha_2}{\Omega} (\dot{\phi}\cos\xi + \dot{\theta}\sin\xi) \right) + \frac{2}{\Omega} (\dot{\phi}\sin\xi - \dot{\theta}\cos\xi), \tag{10}$$

$$\beta_o = \frac{1}{\Omega^2} \frac{n\Omega^2 \rho a c_2{}^2 (B^4 R_2^4 - R_1^4)}{8 I_f} \tag{11}$$

The constants α_1,α_2 are a correction factor to compensate for simplified flybar aerodynamics, $\delta_\phi,\delta_\theta$ are the roll and pitch input command respectively, $\dot{\phi},\dot{\theta}$ are the roll rate and pitch rate of helicopter body frame respectively, ξ is the orientation angle of flybar and $L_{5,6,7,8,9}$ are the linkages in the rotor hub assembly. After substituting the flybar flapping angle of Equation (10) into Equation (6), the equations for the moments M_ϕ, M_θ can be written in the form :

$$\begin{bmatrix} M_\phi \\ M_\theta \end{bmatrix} = \frac{n\rho\Omega^2 acR^4 B^4}{16 L_1 (L_2 + L_3)} \begin{bmatrix} \alpha_3 \frac{L_3 L_8}{L_9} \delta_\theta + C_1 \delta_\theta - C_2 \dot{\phi} + C_3 \dot{\theta} - \alpha_4 L_1 (L_2 + L_3) \frac{\dot{\phi}}{\Omega}) \\ \alpha_3 \frac{L_3 L_8}{L_9} \delta_\phi + C_1 \delta_\phi - C_2 \dot{\theta} - C_3 \dot{\phi} - \alpha_4 L_1 (L_2 + L_3) \frac{\dot{\theta}}{\Omega}) \end{bmatrix} \tag{12}$$

$$C_1 = \alpha_3 L_2 L_4 P_{f1} P_{f2}, \quad C_2 = \alpha_3 L_2 L_4 P_{f1} P_{f3}, \quad C_3 = \alpha_3 L_2 L_4 \frac{2}{\Omega} \tag{13}$$

$$P_{f1} = \frac{n\rho a c_2{}^2 (B^4 R_2^4 - R_1^4)}{8 I_f}, \quad P_{f2} = \frac{\alpha_1 L_7 L_8}{L_5 L_6 L_9}, \quad P_{f3} = \frac{\alpha_2}{\Omega} \tag{14}$$

where C_1, C_2, C_3 are terms from the flybar flapping angle of Equation (8). The C_1 term augments the cyclic input of main rotor and C_2 term increases the damping moment in the helicopter attitude dynamics, which gives control booster to the actuator servo and stabilizing effect to the helicopter respectively. The moment M_ψ around the z-axis is defined by:

$$M_\psi = T_T L_T - K_g r + \tau_m \tag{15}$$

$$T_T = \frac{n}{2} a_T c_T \rho \pi R_T{}^3 \Omega_T{}^2 \left(\frac{B^3}{3}\theta_\psi - \frac{B^2}{2}\lambda_T\right) \tag{16}$$

where T_T is the tail rotor thrust, L_T is the length between the main and tail rotor axes, K_g is the gyro gain for tail rotor, r is the helicopter heading rate, τ_m is the main rotor induced yaw moment in the opposite direction to the tail rotor thrust, defined by:

$$\tau_m = -K_m \delta_o \tag{17}$$

where K_m is the main rotor torque gain, δ_o is the collective pitch cyclic input. The second term in Equation (15) is due to the active yaw damping system in the form of electronic gyro and is described by a simple linear model.

2.3 Overall roll, pitch and yaw attitude dynamics

To simplify dynamics, denoting $\dot{\phi} = p$, $\dot{\theta} = q$, and assuming ρ, a, c, c_1 are constant in Equation (12) and (14) yield the roll model:

$$\dot{p} = k_1 qr + k_2 \delta_\theta - k_3 p + k_4 q + k_{d,1} \tag{18}$$

where:

$$k_1 = \frac{(I_{yy} - I_{zz})}{I_{xx}},\ k_2 = \frac{P_m}{I_{xx}}\left(\frac{\alpha_3 L_3 L_8}{L_9} + C_1\right),\ k_3 = \frac{P_m}{I_{xx}}\left(\frac{\alpha_4 L_1 (L_2 + L_3)}{\Omega} + C_2\right), k_4 = \frac{P_m}{I_{xx}} \mathrm{C}_3 \tag{19}$$

$$P_m = \frac{n\rho ac\Omega^2 R^4 B^4}{16L_1(L_2 + L_3)} \tag{20}$$

The parameters k_1 and k_2 in Equation (18) are considered as the roll torque constant of the main rotor blade angle and the overall effective roll damping respectively. For this model, the parameter $k_{d,1}$ is added as constant external torque offset modelling asymmetry in the roll. It will also account for other unmodelled dynamics.

Similarly, the pitch and yaw rate models are defined:

$$\begin{aligned} \dot{q} &= k_5 pr + k_6\delta_\phi - k_7 q - k_8 p + k_{d,2} \\ \dot{r} &= k_9 pq + k_{10}\delta_\psi - k_{11} r - k_{12}\delta_o + k_{d,3} \end{aligned} \tag{21}$$

where:

$$k_5 = \frac{(I_{zz} - I_{xx})}{I_{yy}},\ \ k_6 = k_2,\ \ k_7 = k_3,\ \ k_8 = \frac{P_m}{I_{yy}} C_3 \tag{22}$$

$$k_9 = \frac{(I_{xx} - I_{yy})}{I_{zz}},\ \ k_{10} = \frac{n}{2} a_T c_T \rho\pi R_T{}^3 \Omega_T{}^2 \frac{B^3}{3},\ \ k_{11} = K_g,\ \ k_{12} = K_m \tag{23}$$

$$k_{d,2} \equiv \text{torque offset in pitch, } k_{d,3} \equiv \text{torque offset in yaw} \tag{24}$$

2.4 Measurement of roll, pitch and yaw

The measurement of orientation angle and attitude velocity are collected using the IMU in an inertial reference frame and body fixed reference frame respectively, which are denoted as quaternion angles and angular rates. The static errors in accuracy of the sensor are $\pm 0.5^o$, which are sufficiently accurate for this application. Note that quaternions are used to calculate the attitude angles to avoid the common problem of gimbal lock with Euler angles, that can cause significant numerical errors.

Therefore, a quaternion representation of attitude is used in the mathematical computation of attitude by integrating the kinematic equation in terms of the unit quaternion vector describing the relation between the rigid body attitude variation and the body angular velocities. The initial conditions are assumed to be zero rotation angle. The quaternions vector $\begin{bmatrix} q_0 & q_1 & q_2 & q_3 \end{bmatrix}$ is solved by the standard set of differential equations:

$$\begin{bmatrix} \dot{q}_0 \\ \dot{q}_1 \\ \dot{q}_2 \\ \dot{q}_3 \end{bmatrix} = \begin{bmatrix} -\frac{1}{2}(q_3 r + q_2 q + q_1 p) \\ \frac{1}{2}(q_2 r - q_3 q + q_0 p) \\ \frac{1}{2}(-q_1 r + q_0 q + q_3 p) \\ \frac{1}{2}(q_0 r + q_1 q - q_3 p) \end{bmatrix} \tag{25}$$

where:

$$\sqrt{q_0^2 + q_1^2 + q_2^2 + q_3^2} = 1, \quad q_0(0) = 1, q_1(0) = 0, q_2(0) = 0, q_3(0) = 0 \tag{26}$$

The time-varying rotational matrix corresponding to the unit quaternion $\begin{bmatrix} q_0 & q_1 & q_2 & q_3 \end{bmatrix}$ is defined as:

$$R_t = \begin{bmatrix} 2(q_0^2 + q_1^2) - 1 & 2(q_1 q_2 + q_0 q_3) & 2(q_1 q_3 - q_0 q_2) \\ 2(q_1 q_2 - q_0 q_3) & 2(q_0^2 + q_2^2) - 1 & 2(q_0 q_1 + q_2 q_3) \\ 2(q_0 q_2 + q_1 q_3) & 2(q_2 q_3 - q_0 q_1) & 2(q_0^2 + q_3^2) - 1 \end{bmatrix} \tag{27}$$

The orientation of the helicopter in terms of the body fixed frame is obtained using the equations:

$$RA = \begin{bmatrix} RAx \\ RAy \\ RAz \end{bmatrix} = Rt * XA_0$$
$$PA = \begin{bmatrix} PAx \\ PAy \\ PAz \end{bmatrix} = Rt * YA_0 \tag{28}$$
$$YA = \begin{bmatrix} YAx \\ YAy \\ YAz \end{bmatrix} = Rt * ZA_0$$

where $XA_0 = [1 \quad 0 \quad 0], YA_0 = [0 \quad 1 \quad 0], ZA_0 = [0 \quad 0 \quad 1]$ are the unit vectors in earth reference frame, RA, PA, YA are the resulting rigid body axis vectors. The angle of body frame axis with respect to earth reference axis is then calculated using trigonometric functions:

$$\begin{aligned} &\phi = \sin^{-1}(r), \quad r = PAz / \cos(\theta) \\ &\theta = \sin^{-1}(RAz) \\ &\psi = \cos^{-1}(RAx / \sqrt{RAx^2 + RAy^2}) \end{aligned} \tag{29}$$

$$\begin{aligned} &\phi \equiv \text{roll angle about RA axis} \\ &\theta \equiv \text{pitch angle about PA axis} \\ &\psi \equiv \text{directional angle about YA axis} \end{aligned} \tag{30}$$

Fig. 4 shows the axes and angles relative to the helicopter body axis, where:

$RA \equiv$ Axis parallel to the tail of helicopter from front nose

$PA \equiv$ Axis pointing directly to the right of helicopter (directly south if the nose is pointing East)

$YA \equiv$ Vertical axis perpendicular to main helicopter blades point down in the formation

The parameters ϕ, θ and ψ in Equation (30) by right hand rule are used to give an intuitive and easily visualized idea of the range of attitude dynamics of the helicopter during flight.

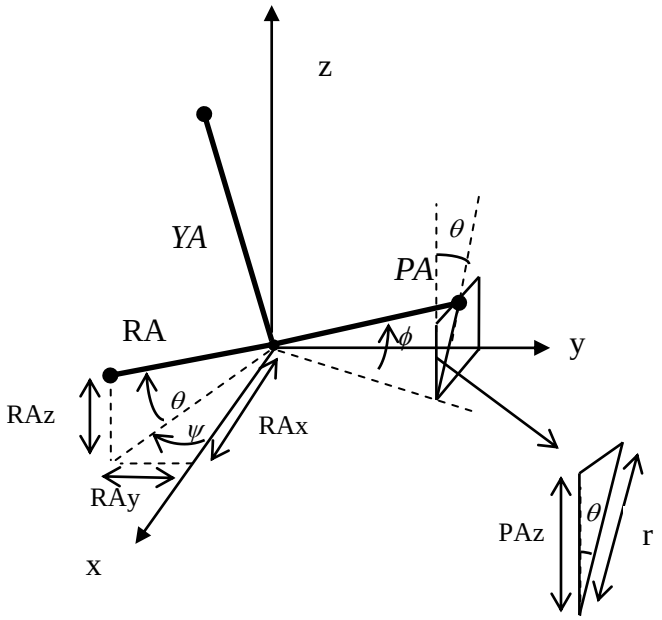

Fig. 4 Angle of helicopter relative to earth reference frame

2.5 Modelling and integral-based parameter identification

2.5.1 Blade cyclic angle (θ_{cyc}) dynamics

The radio controlled servo actuators on the model-scaled helicopter contribute to the overall dynamics due to the servo response time delay. A well known first order approximation to a time delay of τ_i seconds $e^{-s\tau_i}$ is the Pade approximation:

$$\theta_{cyc} + d_1\dot{\theta}_{cyc} = n_1\delta_{cyc} - n_2\dot{\delta}_{cyc} \tag{31}$$

where d_1, n_1, n_2 are the coefficients of Pade approximation.

The approximation of Equation (31) is computed in MATLAB using the *Pade* function. The specific value of τ_i is chosen based on finding the optimal correlation between the commanded angle and the measured roll response. Ideally, the measured angle would be used; however this measurement was not available in the experiment. An advantage of Equation (31) is that it can be easily included as an extra differential equation in the overall model, so it can be easily implemented.

2.5.2 Identifying constant intrinsic parameters

To identify the unknown parameters in Equation (18), the integral-based parameter identification method of [13,14] is significantly extended to handle high sample rates and disturbances. Specifically, the method of [13,14] and other published biomedical papers [19,20] have very low sample rates. Thus, the parameters are identified over regions that have slow dynamics and very little modelling error. For the case of the helicopter, the sample rate is 1000's of times faster, so many other dynamics including disturbances can occur during the time period of parameter identification where parameters are assumed constant. Hence, the methods of [19,20] are not suitable for this application.

For this derivation, it is assumed that the unknown parameter $k_{d,1}$ in Equation (18) is constant for all time. The first step is to define $n+1$ time points, T_i, $i=0,...,n$ that cover the whole data range. These $n+1$ points partition the data into n intervals, $\{[T_{i-1},T_i],\ i=1,...n\}$. For simplicity, each interval is assumed to be the same length. Integrating Equation (18) from T_{i-1} to t yields:

$$p(t) - p_{0,i} = k_1 \int_{T_{i-1}}^{t} qr + k_2 \int_{T_{i-1}}^{t} \delta_\theta dt - k_3 \int_{T_{i-1}}^{t} pdt + k_4 \int_{T_{i-1}}^{t} qdt + k_{d,1}(t - T_{i-1}),$$

$$\mathrm{t} \in [T_{i-1}, T_i), \quad i = 1, ..., n \tag{32}$$

Let $p_{data}(t)$ denote the measured roll rate data and define the function:

$$\begin{aligned} p_{\mathrm{mod}el,i}(t) = p_{0,i} &+ k_1 \int_{T_{i-1}}^{t} q_{data} r_{data} dt + k_2 \int_{T_{i-1}}^{t} \delta_\theta dt \\ &- k_3 \int_{T_{i-1}}^{t} p_{data} dt + k_4 \int_{T_{i-1}}^{t} q_{data} dt + k_{d,1}(t - T_{i-1}) \end{aligned} \tag{33}$$

where:

$$p_{0,i} = p_{data}(T_{i-1}), \quad i = 1, .., n \tag{34}$$

The initial conditions in Equation (34) reset the beginning of each interval to the measured data, which ensures modelling error doesn't build up significantly over time. Choose N equally spaced time points, $\bar{T}_{data,i} = \{T_{i-1} + j\Delta t, \ j = 1, ..., N\}$ in each time interval $[T_{i-1}, T_i), \quad i = 1, ..., n$, with $T_0 = 0$. Setting $p_{\mathrm{mod}el,i} = p_{data}(t)$, for $t \in \{\bar{T}_{data,i}, \ i = 1, ..., n\}$ gives a set of N equations in 5 unknown parameters, which is defined by the matrix equation:

$$\begin{pmatrix} I_1 \\ \vdots \\ I_n \end{pmatrix} X = \begin{pmatrix} \bar{p}_{data,1} \\ \vdots \\ \bar{p}_{data,n} \end{pmatrix} \tag{35}$$

where:

$$I_i = \begin{pmatrix} \int_{T_{i-1}}^{T_{i-1}+\Delta t} qrdt & \int_{T_{i-1}}^{T_{i-1}+\Delta t} \delta_\theta dt & -\int_{T_{i-1}}^{T_{i-1}+\Delta t} pdt & \int_{T_{i-1}}^{T_{i-1}+\Delta t} qdt & (T_{i-1}+\Delta t) - T_{i-1} \\ \vdots & \vdots & \vdots & \vdots & \vdots \\ \int_{T_{i-1}}^{T_{i-1}+N\Delta t} qrdt & \int_{T_{i-1}}^{T_{i-1}+N\Delta t} \delta_\theta dt & -\int_{T_{i-1}}^{T_{i-1}+N\Delta t} pdt & \int_{T_{i-1}}^{T_{i-1}+N\Delta t} qdt & (T_{i-1}+N\Delta t) - T_{i-1} \end{pmatrix}, \quad i = 1, ..., n \tag{36}$$

$$\bar{p}_{data,i} = \begin{pmatrix} p_{data}(T_{i-1} + \Delta t) - p_{0,i} \\ \vdots \\ p_{data}(T_{i-1} + N\Delta t) - p_{0,i} \end{pmatrix}, \quad p_{0,i=} p_{data}(T_{i-1}), \quad i = 1, \ldots, n \tag{37}$$

$$X \in [k_1, k_2, k_3, k_4, k_{d,1}] \tag{38}$$

The integrals in Equation (36) are numerically evaluated using the trapezium rule. An approximation to the unknown parameters X in Equation (38) can be found by solving Equation (35) by linear least squares. Define the resulting parameters of this solution as $\bar{k}_1, \bar{k}_2, \bar{k}_3, \bar{k}_4$ and $\bar{k}_{d,1}$. Due to modeling error and disturbance, these resulting parameters may not be optimal after this first iteration. For the next iteration, define:

$$p_{approx}(t) = p_{approx,i}(t), \quad t \in [T_{i-1,} T_i] \tag{39}$$

$$\begin{aligned} p_{approx,i}(t) = p_{o,i} + \bar{k}_1 \int_{T_{i-1}}^{t} q_{data} r_{data} dt + \bar{k}_2 \int_{T_{i-1}}^{t} \delta_\theta dt \\ - \bar{k}_3 \int_{T_{i-1}}^{t} p_{data} dt + \bar{k}_4 \int_{T_{i-1}}^{t} q_{data} dt + \bar{k}_{d,1}(t - T_{i-1}) \end{aligned} \tag{40}$$

Equation (39) is then substituted back into Equation (35)-(38) to form a new matrix equation. This matrix equation is solved by linear least squares to give new parameters $\bar{k}_1, \bar{k}_2, \bar{k}_3, \bar{k}_4$ and $\bar{k}_{d,1}$, which produce a second approximation $p_{approx,i}(t)$ from Equation (39)-(40). This process is continued until the least squares error between the estimated roll rate $p_{approx}(t)$ and the measured data, changes less than a specified tolerance. The overall algorithm is summarized in Fig. 5. Note that the partitioning of the data into *n* intervals is critical to account for the significant disturbance and high sampling rate in this application. Without this partitioning, the methods previously published in [13,14,19,20] do not perform accurately on the simplified models of Equation (18)-(21), because of

accumulated modelling error on the long stretches of data where the parameters are assumed constant.

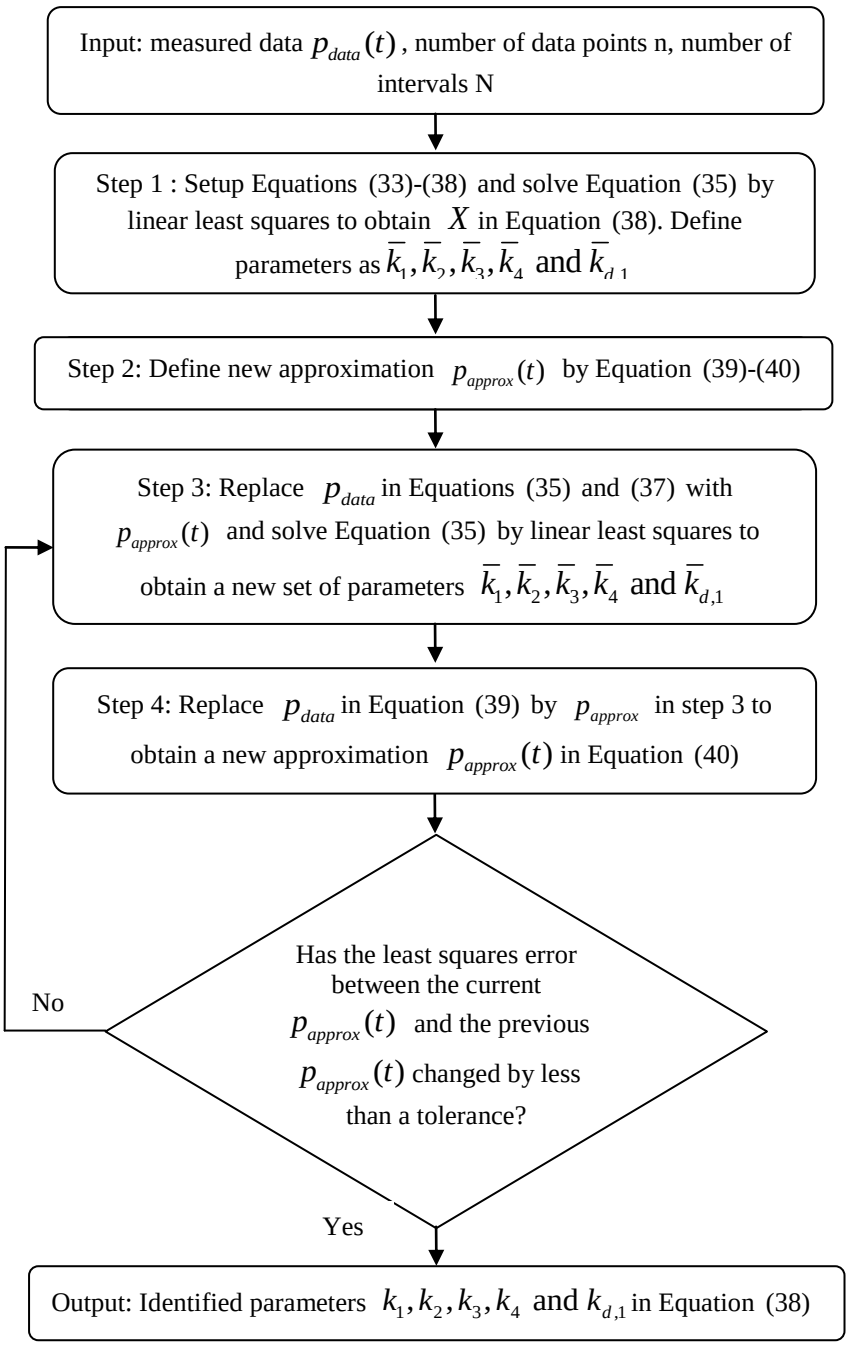

Fig. 5 Algorithm of integral method

2.5.3 Modeling wind disturbance

The helicopter was flown outdoors, thus environment disturbance has a significant effect on the dynamics. Wind disturbance models are common in the literature, but they typically only deal with one type of disturbance, for example vertical wind gusts [21].

The approach in this paper is to capture the complex disturbance directly by computing the effective applied torque to the helicopter at discrete intervals. The applied wind load is modeled as the constant cyclic input command required to reproduce the observed helicopter response for the given time period. The model is defined by:

$$\dot{p}(t) = k_1 q(t) r(t) + k_2 \delta_\theta(t) - k_3 p(t) + k_4 q(t) + \bar{u}_d(t) \tag{41}$$

$$\bar{u}_d = k_2 u_d(t) + k_{d,1} \tag{42}$$

In Equation (41), the constant values of k_1, k_2, k_3 and k_4 are assumed known or estimated and the effect of the mean wind speed, wind fluctuations and the roll offset are lumped into single parameter $\bar{u}_d$, which is defined:

$$\bar{u}_d(t) = \sum_{i=1}^{n} (H(t-(i-1)\Delta t) - H(t-i\Delta t))\bar{u}_{d,i} \tag{43}$$

$$\begin{aligned} H(t) &= 1, \quad t > 0 \\ &= 0, \quad t < 0 \end{aligned} \tag{44}$$

where $H(t)$ is the Heaviside function and Δt is the specified time interval that $u_d(t)$ is assumed to be constant over. With this formulation in Equation (41), the disturbance $u_d(t)$ is a meaningful parameter as it relates the external disturbance to a torque $\bar{u}_d(t)$. This torque can be written in terms of the equivalent cyclic input $u_d(t)$ and a constant disturbance offset $k_{d,1}$ in Equation (42). This approach

allows virtual profiles of the observed disturbances to be stored and used later for control development.

Once k_1, k_2, k_3, k_4 and $k_{d,1}$ are identified using the algorithm of Fig. 5, the piecewise constant $\bar{u}_d(t)$ in Equation (43) is identified over the intervals of length Δt. The choice of Δt can significantly affect the model match and identified disturbance profile. If Δt is too large, the disturbance profile will not capture any high frequency wind inputs. If Δt is too small, it will capture a large amount of noise. For simplification of implementation, Δt is chosen based on the data logging frequency.

To account for noise, the identified disturbance profile is smoothed a number of times by a 10 point moving average. The numbers of smoothings is chosen to give a fitted normal distribution that is the closest least squares match to the fitted normal distribution of the blade cyclic command. The assumption is that the variations in the blade cyclic command about the mean are approximately correlated to the wind loads on the roll axis. This assumption is reasonable as the test pilot is manually keeping the helicopter stable in the roll via a joy stick and radio control. If a large wind disturbance moves the helicopter in the roll, the test pilot will move the blade cyclic angle a lot faster and further than for the case of a small disturbance.

Let $\bar{N}$ be the number of time intervals of width Δt that fit in the whole time period of the experiment, and

$$t_i = i\Delta t, \qquad i = 1, \ldots, \bar{N} \tag{45}$$

Integrating Equation (41) from t_{i-1} to t, yields:

$$p(t_i) - p(t_{i-1}) = \int_{t_{i-1}}^{t} (k_1 q(t) r(t) + k_2 \delta_o(t) - k_3 p(t) + k_4 q(t) +) dt + \bar{u}_{d,i}(t - t_{i-1}) \tag{46}$$

where $\bar{u}_{d,i}$ is an unknown constant. Solving Equation (46) for $\bar{u}_{d,i}$ yields:

$$\bar{u}_{d,i} = k_2 u_{d,i} + k_{d,1} \tag{47}$$

Once $\bar{u}_{d,i}$ in Equation (47) is known, $u_d(t)$ and $k_{d,1}$ in Equation (42) can be determined from the known value of k_2 and an assumption that $u_d(t)$ has a mean value of zero.

2.6 Extended Kalman Filter Method

The Extended Kalman filter (EKF) is a recursive algorithm that produces an estimate of states and an estimation error covariance. It requires a measured output, a known input and system model, and the assumed process and measurement noise statistics. The goal is to characterize the ability of an EKF to identify the unknown parameters of Equation (18). To simplify analysis, the parameters k_1 and k_4 in Equation (18) are set to zero. The continuous-time model of Equation (18) is discretized using a simple Euler integration scheme, with sample time $T_s = 22\text{ms}$, corresponding to the data logging frequency of 45Hz. The discrete model is defined as:

$$p_{k+1} = p_k + T_s(-k_1 p_k + k_2 u_k + k_d) + w_k \tag{48}$$

where subscript k is the discrete time index and $p_k = p(t_k)$. In the time interval $[t_k, t_{k+1}]$, the input u_k is assumed constant, w_k is the state noise process due to disturbance and modelling error, and is assumed to be zero-mean, white Gaussian noise with variance Q.

The unknown parameters k_1, k_2 and k_d in Equation (48) are estimated by treating the parameters as state variables, which renders the estimation problem effectively nonlinear [22]. The unknown parameter vector is defined by:

$$\Theta = \{k_1, k_{2,} k_d\}^T \tag{49}$$

The constant system parameter Θ is considered as the output of an auxiliary dynamic system:

$$\dot{\Theta} = 0 \tag{50}$$

Thus, the augmented state vector is defined by:

$$\bar{x} = \begin{bmatrix} p \\ \Theta \end{bmatrix} \tag{51}$$

The augmented state equation is represented by:

$$\bar{x}_{k+1} = F(\bar{x}_k, u_k) + \Gamma w_k \tag{52}$$

$$\Gamma = \begin{bmatrix} I_{1\times 1} \\ \mathbf{0}_{3\times 1} \end{bmatrix}, \quad \mathbf{0}_{3\times 1} \equiv \text{zero matrix}, \; F(\bar{x}_k, u_k) = \begin{Bmatrix} T_s(-k_1 p_k + k_2 u_k + k_3) \\ \Theta_k \end{Bmatrix} \tag{53}$$

Since the only roll rate is considered, the observation equation is:

$$z_k = p_k \cong H x_k + v_k \tag{54}$$

where v_k is zero-mean white Gaussian noise with variance R corresponds to measurement error. The augmented observation equation is:

$$z_{k+1} = \begin{bmatrix} H_{1\times 1} & \mathbf{0}_{1\times 3} \end{bmatrix} \begin{bmatrix} x_{k+1} \\ \Theta_{k+1} \end{bmatrix} + v_{k+1} = \bar{H}\bar{x}_{k+1} + v_{k+1} \tag{55}$$

The EKF approximates the nonlinear filtering problem by linearizing the model of Equation (52) at each time step around the last best estimate of the nonlinear process $\bar{x}_k^*$,

$$\bar{x}_{k+1} = F(\bar{x}_k^*, u_k) + \frac{\partial F(\bar{x}_k^*, u_k)}{\partial \bar{x}}(\bar{x}_k - \bar{x}_k^*) + O(2) + \Gamma w_k \tag{56}$$

where:

$$\frac{\partial F(\bar{x}_k^*, u_k)}{\partial \bar{x}} = \begin{bmatrix} I_{1\times 4} + \frac{\partial F(\bar{x}_k, u_k)}{\partial \bar{x}} T_s \\ \mathbf{0}_{3\times 1} \quad \mathbf{I}_{3\times 3} \end{bmatrix} \tag{57}$$

The second highest order term is very small and hence ignored. The discrete time state transition matrix of Equation (57) is denoted by $\bar{\Phi}(\bar{x})$. $(\sim)$ and $(\wedge)$ is used to denote the predicted and corrected variables respectively.

Extrapolation:

$$\tilde{x}_{k+1} = \hat{x}_k + F(\hat{x}_k, \hat{\Theta}_k, u_k)T_s \tag{58}$$

$$\tilde{\Theta}_{k+1} = \hat{\Theta}_k \tag{59}$$

$$\tilde{P}_{k+1} = \Phi \hat{P}_k \Phi^T + \Gamma \mathbf{Q} \Gamma^T \tag{60}$$

$\sim \equiv$ predicted variable, $\wedge \equiv$ corrected variable (61)

Update:

$$K_{k+1} = \tilde{P}_{k+1} \bar{H}^T (\bar{H} \tilde{P}_{k+1} \bar{H}^T + R)^{-1} \tag{62}$$

$$\hat{x}_{k+1} = \tilde{x}_{k+1} + K_{k+1}(z_{k+1} - \bar{H}\tilde{x}_{k+1}) \tag{63}$$

$$\hat{P}_{k+1} = (I_{4\times 4} - K_{k+1}\bar{H})\tilde{P}_{k+1} \tag{64}$$

3 RESULTS AND DISCUSSION

3.1 Test Data Pre-processing

The servo actuation signals collected during the experiment are the time interval of pulse width modulation (PWM) and are in milliseconds. Because of the electronic mixing feature on the RC helicopter, all three servo motors around the swashplate work together to achieve the desired pitch angle on the main rotor blade. Therefore, the control inputs (longitudinal cyclic, lateral cyclic, collective and pedal) from the pilot stick are not related to the three servo motors on one-to-one basis except the pedal input. In order to correlate the control inputs to the four servos PWM signal, an experiment is perfomed and a linear correlation is assumed. The predefined equation is:

$$\begin{bmatrix} U_{AILE} \\ U_{AUX} \\ U_{ELEV} \\ U_{RUDD} \end{bmatrix} = G * \begin{bmatrix} \delta_{lon} \\ \delta_{lat} \\ \delta_{col} \\ \delta_{ped} \end{bmatrix} \tag{65}$$

where $\begin{bmatrix} U_{AILE} & U_{AUX} & U_{ELEV} & U_{RUDD} \end{bmatrix}^T$ are the four servo motor signals pulse width measurement, $\begin{bmatrix} \delta_{lon} & \delta_{lat} & \delta_{col} & \delta_{ped} \end{bmatrix}^T$ are the pilot sticks adjustment range (± 1 for $\delta_{lon}, \delta_{lat}, \delta_{ped}$ and δ_{col}). After substituting the obtained data from a few combinations of control input with a corresponding PWM signal, the resulting formula is obtained:

$$\mathbf{U} = \mathbf{G}' * \delta + \mathbf{U}_{trim} \tag{66}$$

where $\mathbf{U}_{trim}$ is the pulse width for starting position of pilot stick position, $\mathbf{G}'$ is the determined control input gain. In order to access the control input at any time, the following equation translates the servo motors pulse width to the corresponding control input:

$$\delta = \mathbf{G}'^{-1}(\mathbf{U} - \mathbf{U}_{trim}) \tag{67}$$

Fig. 6 shows the control input plot after conversion from the servo motor measurement for the first 50s. To further show the frequency range of the input excitation, a Fast Fourier Transform (FFT) plot for each control input is given in Fig. 7. The control inputs in Fig. 6 and Fig. 7 include purposely constructed oscillation as well as the natural pilot response to mitigate wind gusts on the helicopter. This inputs cover a good range of excitation frequencies for identifying the major attitude dynamics in each axis. In addition, Fig. 6 shows that prior to the significant actuation input from the pilot, the helicopter is held as close as possible to the steady state given the gusty wind conditions.

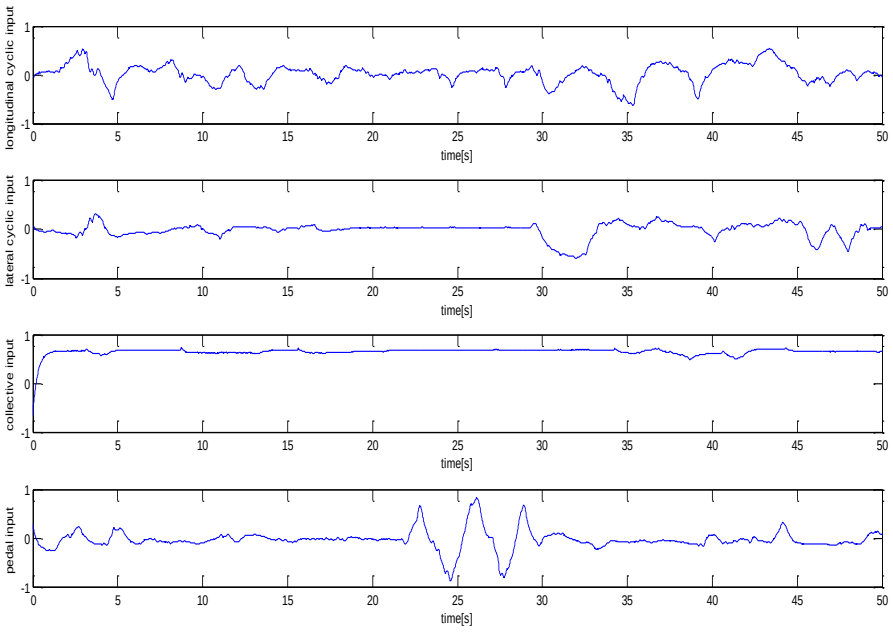

Fig. 6 Control input plot

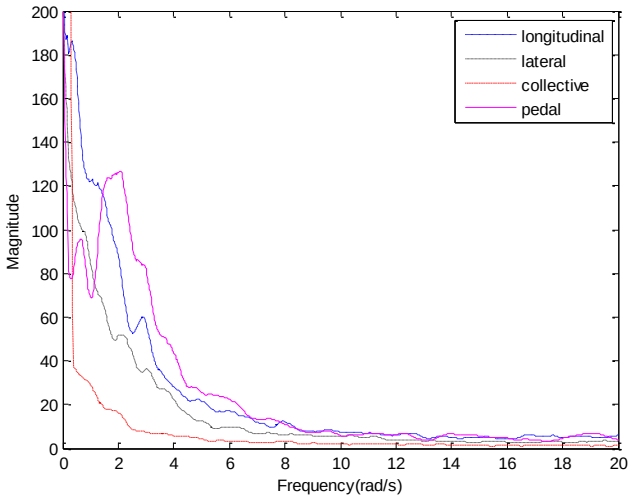

Fig. 7 FFT plot of control inputs

Fig. 8(a) shows an example of the measured angular roll rate, which is quite noisy. The noise is likely due to the large amount of vibration transferred from the airframe to the sensor since there is no such noise in the control inputs of Fig. 6. To reduce this noise and allow a more suitable comparison to the model, a finite impulse response (FIR) low pass filter is implemented in Matlab. The cutoff frequency of passband and stopband are set at 4*Hz* and 8*Hz* respectively which is more than covers the observed frequencies in the control input. Fig. 8(b) gives an example of the smoothed profile.

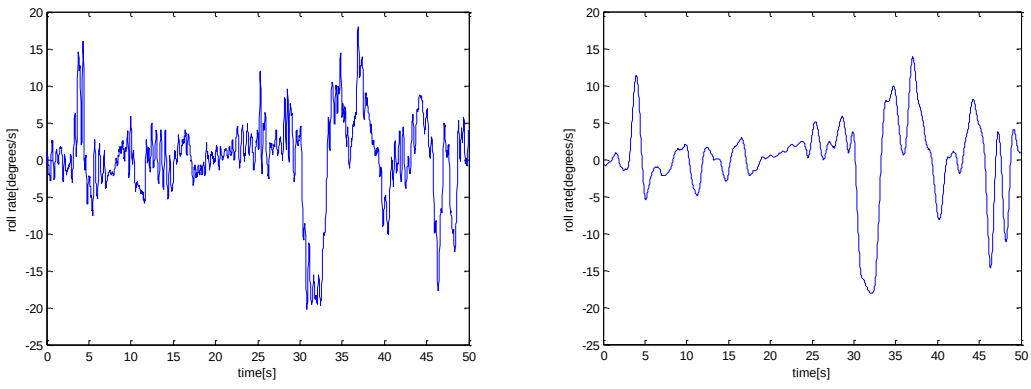

Fig. 8 (a) Measured roll rate. (b)Smoothed measured roll rate

3.2 Integral-based identification for roll dynamics identification

The algorithm of Fig. 5 is now applied to the roll rate data in Fig. 8(b) with $k_1 = 0, k_4 = 0$. The resulting parameters are:

$$k_2 = 1.3475\ , \quad k_3 = 2.4208\ , \quad k_{d,1} = 0.0399 \tag{68}$$

These parameters and $k_1 = 0, k_4 = 0$ are substituted into the model differential Equation (18) and numerically simulated using ode45 in Matlab. Fig. 10 gives a close up of two regions in Fig. 9, which shows a good overall match. Fig. 11 shows in detail the difference between the measured and modelled roll rate. The algorithm of Fig. 5 is now applied to the pitch rate and yaw rate data with coupling terms set to zero, the resulting parameters are:

$$k_6 = \text{-}0.8903\ , \quad k_7 = 2.5188\ , \quad k_{d,2} = 0.0115 \tag{69}$$

$$k_{10} = 13.4702\ , k_{11} = 3.4342\ , k_{12} = \text{-}0.5623,\ k_{d,3} = 0.0964 \tag{70}$$

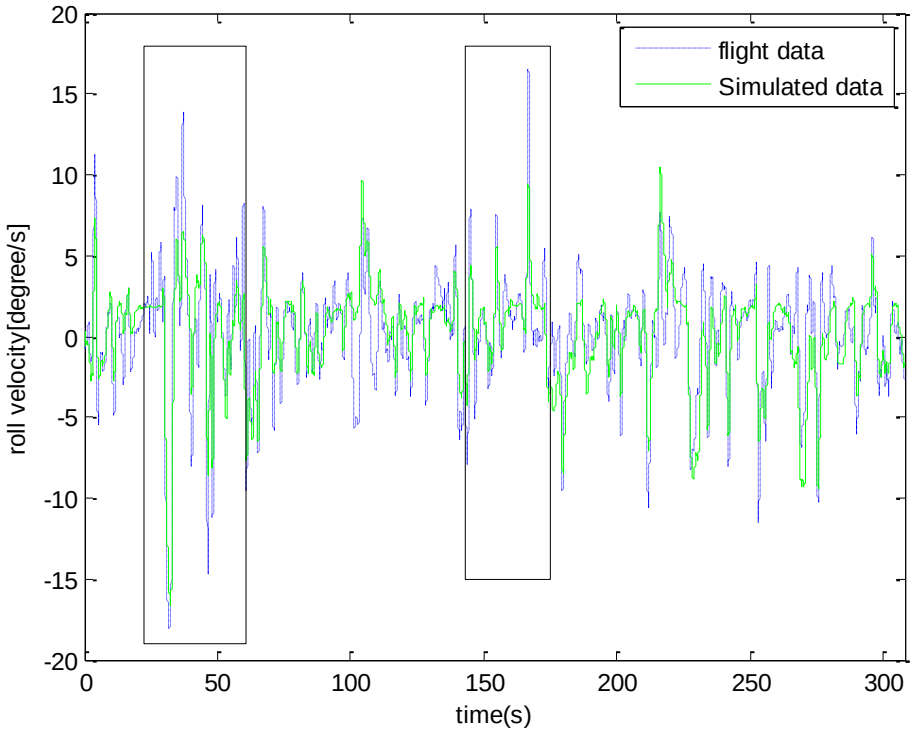

Fig. 9 Integral-based roll rate estimation compared with flight data

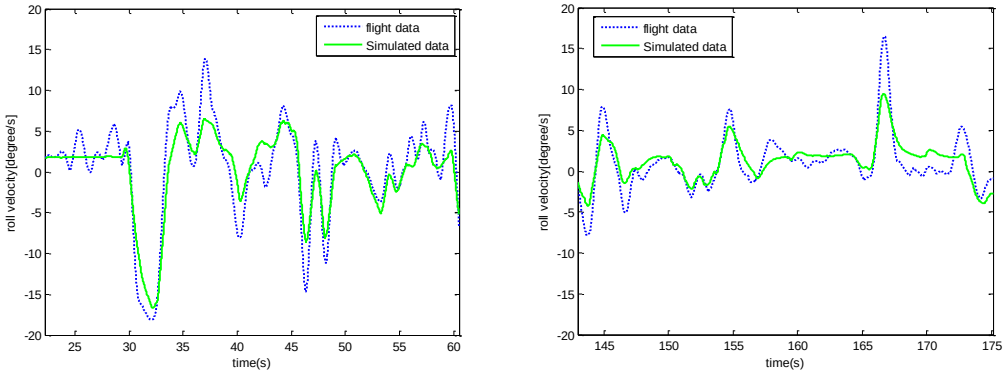

Fig. 10 (a) Close-up region R1 in Fig. 9 (b) Close-up region R2 in Fig. 9.

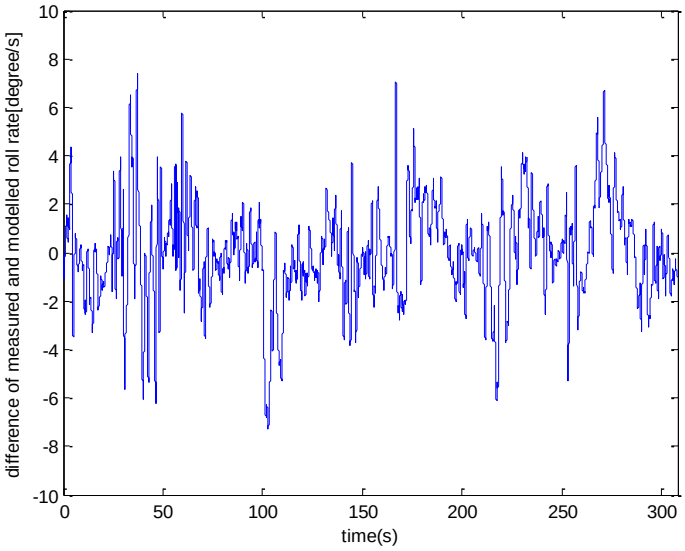

Fig. 11 The difference between the measured and modelled roll rate

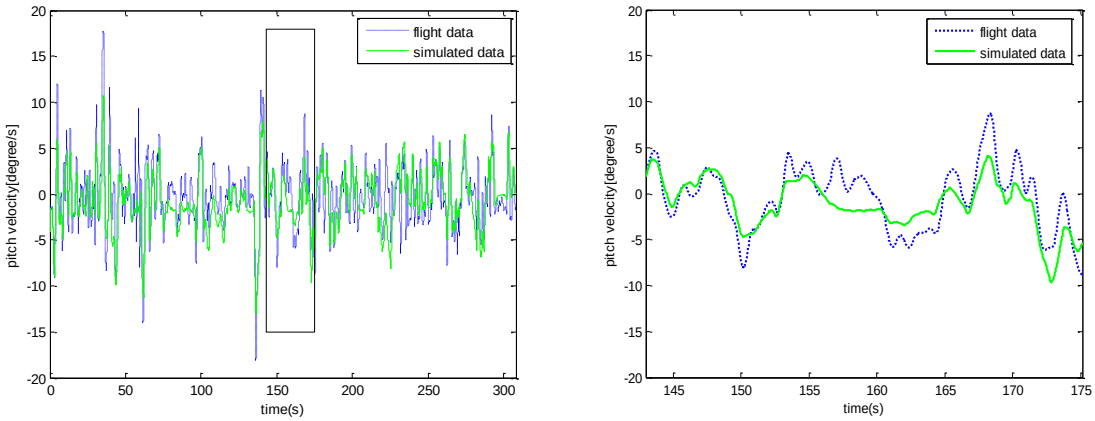

Fig 12 Integral-based pitch rate estimation compared with flight data at certain time interval

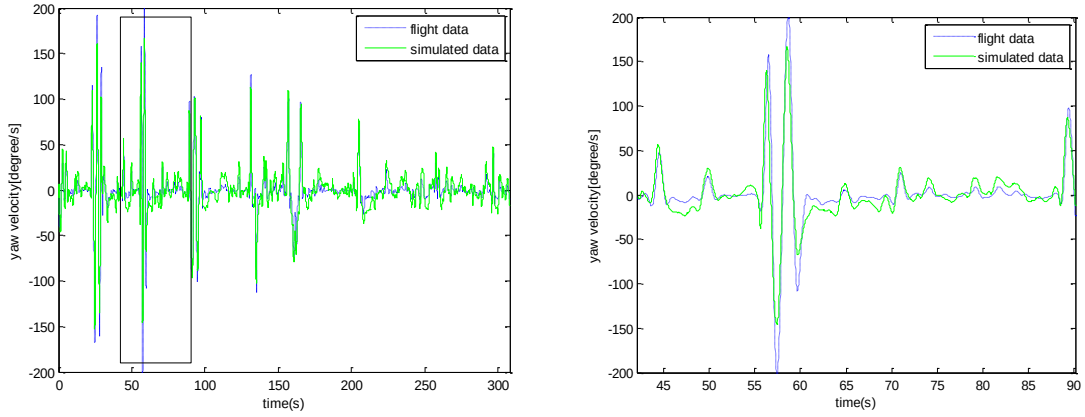

Fig. 13 (a) Integral-based yaw rate estimation compared with flight data. (b) Close-up region R1 in (a)

The mean absolute error and the 90th percentile of the attitude rate in degrees/s are given in Table. 1. The error of the attitude rate relative to the maximum absolute attitude rate is also shown. Note that yaw rate has significantly larger errors than the roll rate and pitch rate, but this increased error is due to the much higher yaw rate observed and it has lower relative percentage error.

Attitude	Mean absolute error(degree/s)	90^{th} percentile(degree/s)	Error relative to maximum (%)
Roll rate	1.5166	2.5152	8.39
Pitch rate	1.7444	3.1993	9.68
Yaw rate	7.7574	11.9200	3.83

Table. 1 Error statistics of helicopter roll rate, pitch rate and yaw rate

As a further comparison the parameters $k_1,...,k_{12}$ in Equations (18)-(24) are identified using the integral method. For example, in the roll rate, the parameters are identified by substituting the measured q and r and applying the algorithm in Fig. 5. A similar method is applied to the pitch and yaw rates. Once the parameters are identified, Equations (18)-(24) are solved numerically and the resulting response is compared to the measured data. Fig. 14 gives a comparison between the coupled model response, the decoupled model response of Fig. 10 and the measured data. These results further show the capabilities of the integral method to identify more complex models. It also shows that in this case there is little gain in using the complex model of Equations (18)-(24) over the simplified models. The full comparison is given in Table. 2. The results show that the more complex model has a slightly lower mean absolute error compared to the simpler model. From the result, it can be seen that the coupling terms have very little effect on the overall attitude dynamics since any potential benefit is swamped by wind disturbance.

Attitude	Mean absolute error(degree/s) coupled model	Mean absolute error (degree/s) between models	90th percentile(degree/s)	Error relative to maximum (%)
Roll rate	1.4927	0.0064	2.4578	8.25
Pitch rate	1.6266	0.0138	2.7739	9.03
Yaw rate	7.8203	0.0168	12.2085	3.86

Table. 2 Error statistics of helicopter roll rate, pitch rate and yaw rate of coupled model and mean absolute error of between models

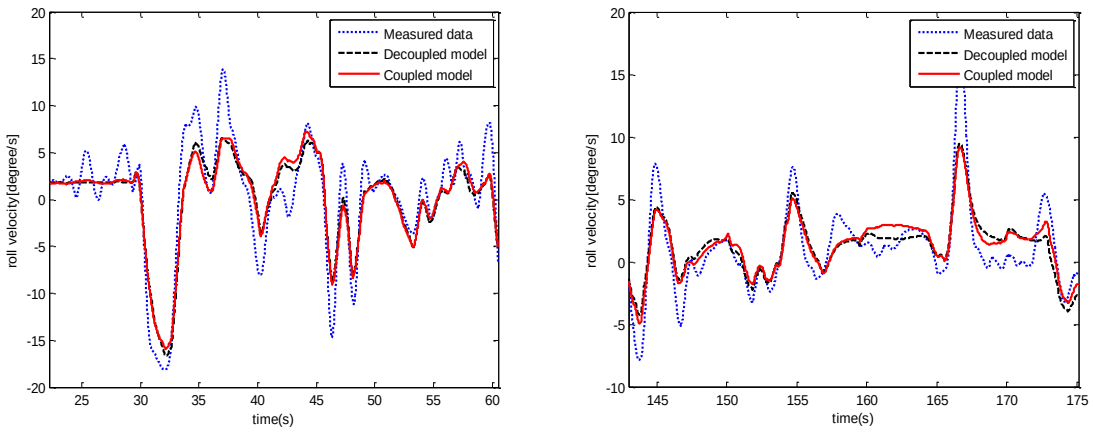

Fig. 14 Comparison of roll rate between measured data, decoupled model and coupled model

In order to further validate the dynamics model, the modelled predicted ϕ, θ and ψ of the helicopter are computed from Equations (25)-(29). To remove drift in integration, the best least squares piecewise linear function over 10s periods is subtracted from the data and the model using the command "detrend" in matlab. The resulting detrended modelled and measured angles are plotted in Fig. 16,17 and 18. As a further comparison to complement Fig. 16, the residual error between the measured and quaternion derived roll angle is shown in Fig. 15. The results show that the minimal model captures all the major attitude dynamics quite

accurately. Specifically, the modelled roll angle tracked the measured angle with a mean absolute error of 1.7860 degrees and a standard deviation of 2.4779 degrees. For the pitch angle, the mean absolute error is 2.1029 degrees and standard deviation is 3.0539 degrees. For the yaw angle, it has a mean absolute error of 6.8740 degrees and standard deviation of 8.9974 degrees. Note that some of the precise quantitative variations are not captured since there was significant wind gusts during the experiment and no disturbance is included in this model response.

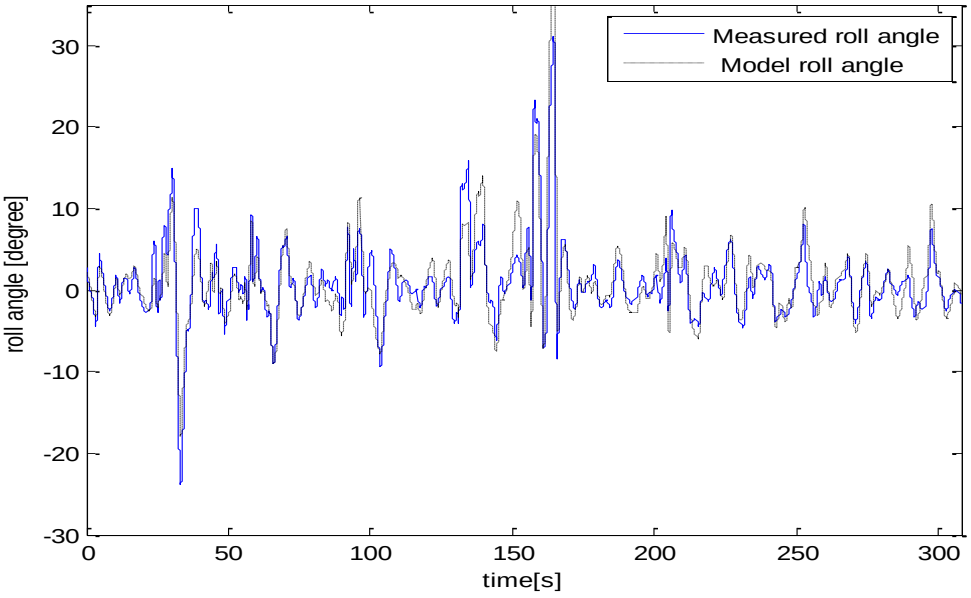

Fig. 16 Measured roll angle vs quaternion derived roll angle

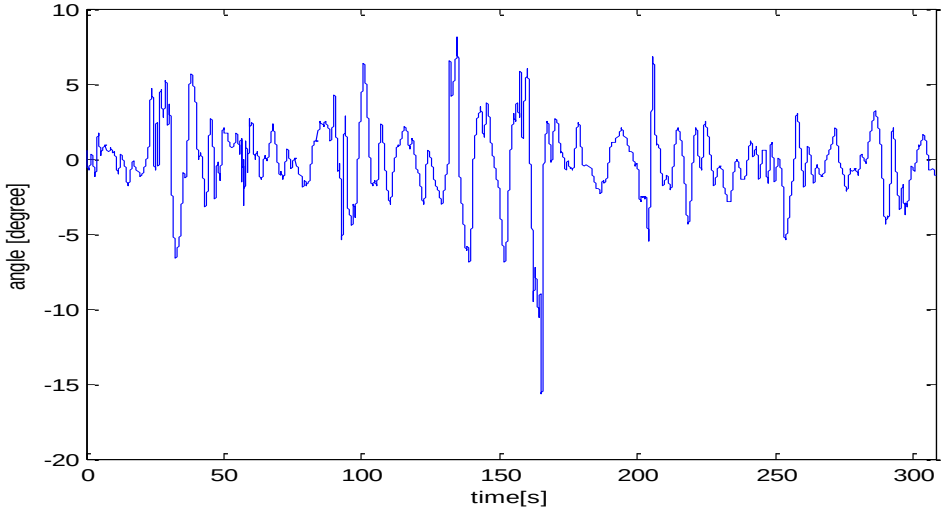

Fig. 15 Residual error between measured and model angle

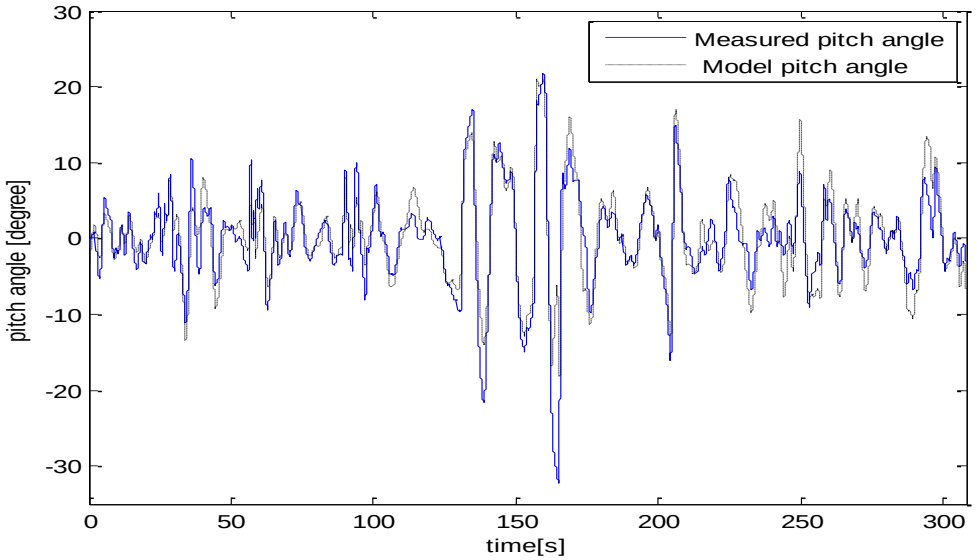

Fig. 17 Measured pitch angle vs quaternion derived pitch angle

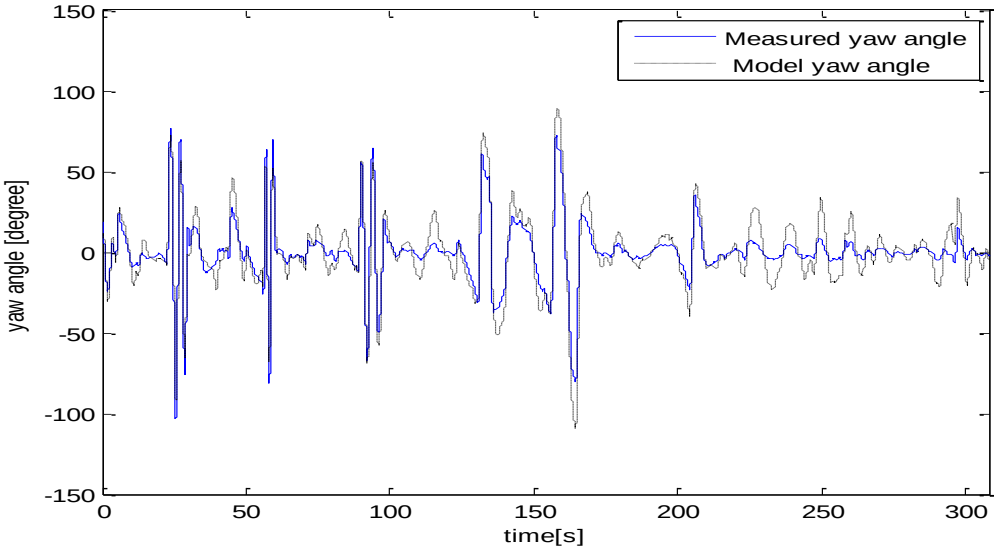

Fig. 18 Measured yaw angle vs quaternion derived yaw angle

3.3 Identification of external disturbance $u_d(t)$ on helicopter roll dynamics

The helicopter roll response with external disturbances present is modelled by Equation (41), where $k_1 = 0, k_4 = 0, k_2, k_3$ are assumed to be known and $p(t)$ and δ_θ are directly measured. Fig. 19 shows the disturbance profile u_d after applying Equation (46) for identifying the time varying disturbance. Note that a 10-point moving average is applied 5 times to disturbance profile. The 5 times smoothing is chosen to minimize the least square error between the best fitted normal distributions of the pilot control input and the disturbance respectively, which are shown Fig. 20 and Fig. 21. The assumption is that the wind inputs are roughly equivalent to the pilot's input to try and repel the disturbance.

For further validation of this approach, the Kolmogorov-Smirnov test is applied to the similarities of both distributions. From the test, a p-value of 0.00097 is obtained, which shows that both normal distributions of the input and disturbance are statistically similar. In addition, the 90% confidence interval of u_d is [-0.0829, 0.0901], whereas for the cyclic input the [-0.1539, 0.0543]. This result shows that the smoothed disturbance profile is within the same range as the pilot control inputs so is physically realistic and is thus a reasonable representation of the wind disturbances in the test. For example, if a disturbance was identified with a value greater than what is physically possible with the control inputs, it suggests that the model is over fitted and not valid. Hence this approach of comparing fitted distributions is a consistent way of identifying a realistic disturbance profile that could be used for later control development.

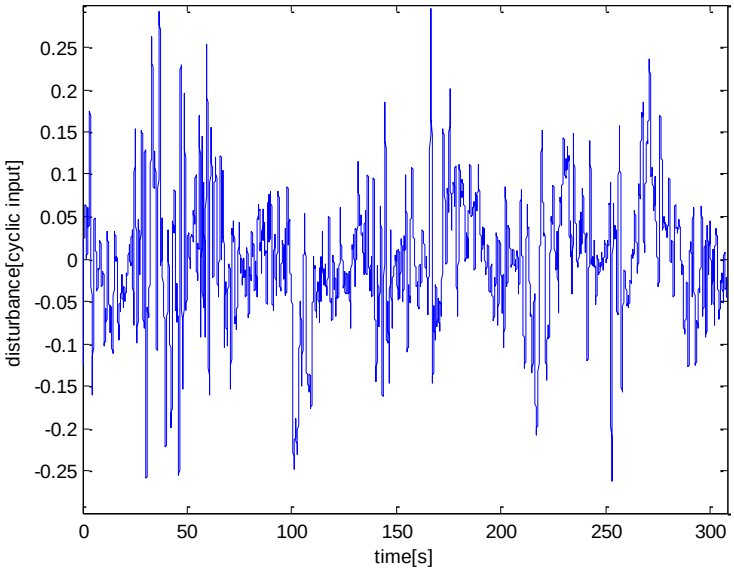

Fig. 19 Identified roll rate disturbance

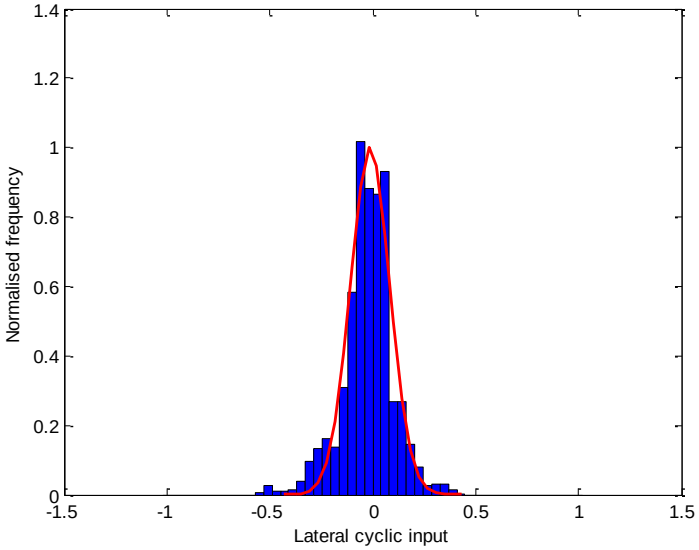

Fig. 20 Histogram of pilot control input

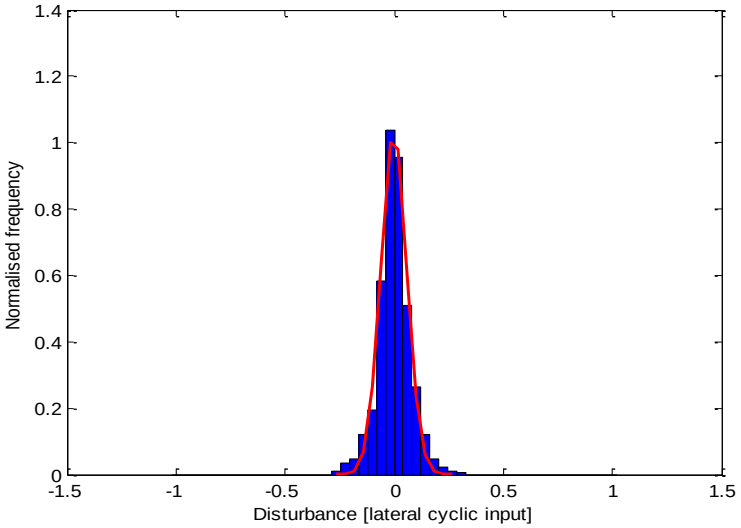

Fig. 21 Histogram of disturbances

3.4 Simulating model with disturbances

Using the identified disturbance $u_d(t)$ from Equation (42) and the parameters from Equation (18) with $k_1 = 0, k_4 = 0$, the model of Equation (41) describing the roll dynamics is numerically solved and compared to the measured roll rate. The modelled roll rate predicted the measured roll rate with mean absolute error of 0.0953 degrees/s and standard deviation of 0.1322 degrees/s. In addition, the quaternion roll angle found from using Equations (25)-(29) is compared to the measured quaternion roll angle. The modelled roll angle tracked the measured roll angle with a mean absolute error of 0.2793 degrees and standard deviation of 0.1947 degrees. Importantly, these accurate results are obtained with a realistic disturbance model representing the significant wind fluctuations.

3.5 Computation speed evaluation

To show the significant computation efficiency of the integral method, a comparison is made to standard non-linear regression (NLR) in MATLAB. Both methods are implemented on a laptop equipped with 2.50GHz CPU and 3.98GB of RAM. In the NLR method, the objective function for Equation (18) is defined:

$$F(k_1, k_2, k_d) = \sum_{i=1}^{N} (p_{numerical}(k_1, k_2, k_d)(t_i) - p_{data}(t_i))^2 \tag{71}$$

$$p_{numerical} \equiv \text{ numerical solution of Equation (18)} \tag{72}$$

The numerical solver chosen is ode45 and the absolute and relative tolerances that control the automatic step size are increased until the error in simulation reaches a maximum of 5% with respect to the most accurate solution obtained from using a very small step size. This approach ensures the simulation speed is made as fast as possible to provide an accurate computational comparison. The command *lsqnonlin* in Matlab is used to find the unknown parameters k_1, k_2 and k_d that produce the best least squares solution to Equation (71). The starting point for the parameters is set as:

$$k_1 = 5, \quad k_2 = 5, \quad k_d = 5 \tag{73}$$

The results are shown in Table. 3. It can be seen that integral method is approximately 710 times faster than the NLR method, and has very similar accuracy. The reason for such a significant speed increase is that the integral method only requires sums of data which are very fast to compute and most importantly it does not require any forward simulation at each iteration. The nonlinear regression requires the solution of the underlying differential equation at each iteration which is very computationally expensive. Similar gains have been observed in the bio-medical field [13] .

	CPU Time(s)	Mean Absolute error(degree/s)
Integral Method	~ 0.63	1.5261
NLR [5,5,5]	~ 447.80	1.3913
NLR [50,50,50]	~688.00	2.4547
NLR [100, 100,100]	~ 380.06	55.7191

Table. 3 Comparison between Integral method and NLS

Table. 3 also shows two cases where the starting points are set far away from the solution. One of these cases has significant error, showing that in this case the NLR method has found a local minima. Therefore, there is no guarantee in finding the global minima unless the starting point is near to the solution. This result shows the typical starting point dependence of NLR, which increases the computation time further when several other starting points have to be used. The integral method uses the measured data as starting point so does not require a good initial starting point for the parameters.

3.6 EKF Identification method

Using Equation (18), the nonlinear model is discretized and linearized at each sample point and the states and unknown parameters are estimated following EKF algorithm in Equations (58)-(64). Before applying the EKF method, estimates of the state covariance, the initial parameter and noise statistics are required [18]. A priori knowledge on the model parameters were initially obtained based on the

integral method result so that the initial state covariance $\tilde{p}(0)$ could be set to a low value. Specifically, the values used were:

$$\tilde{\mathbf{p}}(0)=\begin{bmatrix} 1e\text{-}2 & 0 & 0 & 0 \\ 0 & 1 & 0 & 0 \\ 0 & 0 & 1 & 0 \\ 0 & 0 & 0 & 1 \end{bmatrix} \tag{74}$$

The noise statistics were determined empirically using a grid search on a wide range of possibilities to find the best match between the simulated roll rate and measured roll rate. This approach ensures that a global optimum value was found. In order to keep track of the growth in uncertainties in the estimation procedure, covariance analysis is performed by following the changes in diagonal elements of the covariance matrix $\hat{P}$ [23]. This process is illustrated in Fig. 22, where it shows the analysis for the case 3(a) in Table. 4 below. The uncertainties are slowly stabilizing to constant values and do not grow unboundedly. Fig. 23 shows the estimated parameters in roll dynamics that converge to stable value. The resulting error in the roll rate prediction is shown in Table. 4.

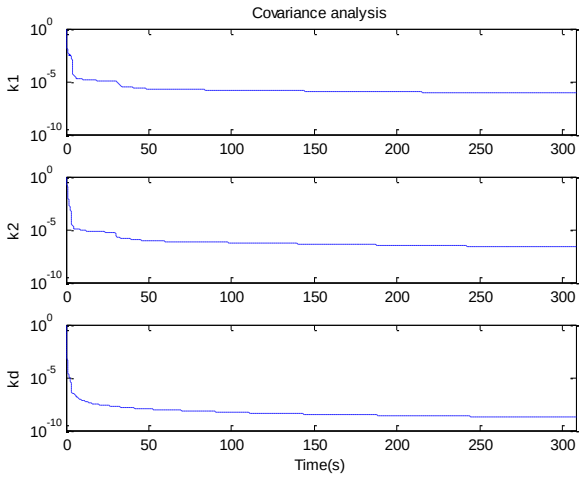

Fig. 22 Covariance analysis of the estimated parameters $k_1,\ldots,k_d$

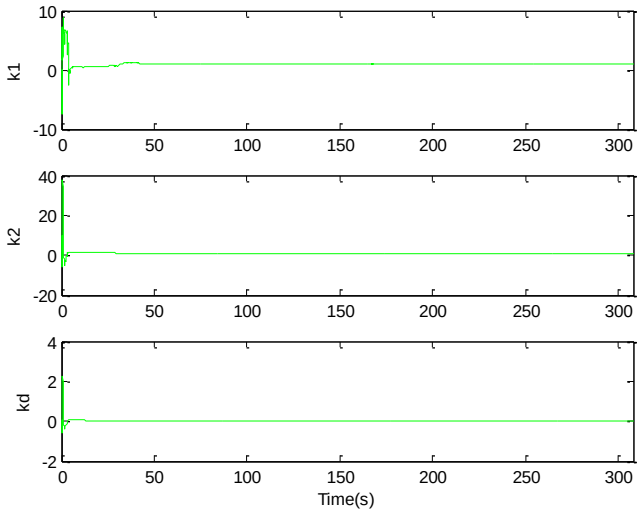

Fig. 23 parameters estimation result for $k_1,...,k_d$

The results show that with optimal estimate on state covariance, initial parameters and noise statistics, the EKF can estimate the roll rate satisfactorily. However, the computation time required to obtain this estimate was 2.5178s for 308s of roll rate data, which is ~ 30 times slower than the integral method but faster than the non-linear regression method. In addition, the error is nearly 2 times greater than the integral method and non-linear regression method. Hence for the EKF method, even in the best case where optimal noise statistics are known, there is still a trade-off between an increase in speed and a loss of accuracy. The integral method does not have this problem.

However, a further difficulty with the EKF identification method is that it can be very dependent on the process noise covariance matrix Q_c and the initial states [24]. To illustrate this sensitivity, three main cases are considered as shown in Table. 4. Note that the parameter m_o is a vector comprising the initial roll rate value and 3 unknown parameters in roll dynamics equation.

	m_o	Q	Mean Absolute Error(degree/s)	90th percentile (degree/s)
Case 1(a)	[0 0.1 10 0.1]	1	73.9202	142.2668
Case 1(b)	[0 2 3 0]	1	4.3078	7.6458
Case 2(a)	[0 0.1 10 0.1]	1e-8	2.2244	3.6727
Case 2(b)	[0 2 3 0]	1e-8	2.2289	3.6708
Case 3(a)	[0 0.1 10 0.1]	1e-2	3.9678	6.8241
Case 3(b)	[0 2 3 0]	1e-2	2.2884	3.7996

Table. 4 Error statistic for roll rate from EKF method

Cases 1 and 3 show that for a suboptimal value of Q the error is very sensitive to the initial state m_o. However, for an optimal value of Q, case 2 shows that the results are not significantly affected by the initial state m_o. The value of Q is essentially equivalent to the amount of modeling error which is highly dependent on the wind conditions on the day and other helicopter dynamics which are highly variable. Thus, to ensure a globally optimal value of Q is chosen, there will always be some simulations of the numerical solver ode45 required which would significantly further slow down the computation. Furthermore, since the best solution that the EKF could achieve has twice the error of the non-linear regression and the integral method approaches, it appears to be not suitable for this type of application, where significant disturbances are present. These large disturbances are due to the helicopter being flown outdoors.

Further testing on the rate of parameter convergence of EKF found that even when the optimal value of Q is chosen and initial parameters are set as in case 3(a) in Table. 4, estimation of the unknown parameter value using EKF appears to be very slow. The results are shown in Table 5 with 3 different data

sample length. In case 1, the parameters are not fully converging to the true value which results in poor prediction of roll response. As the sample length increased beyond 10s, the mean absolute error decreases to a level that similar to the error in Table. 4, which implies that the parameters are close to converging. However, the integral method does not have this problem, as the parameters converge immediately on any time period. Thus, the integral method has an additional advantage over the EKF in terms of tracking fast changes in the helicopter parameters in real time in the presence of significant disturbance.

	Sample time period(s)	**Mean Absolute Error(degree/s)**	**90^{th} percentile (degree/s)**
Case 1	4.84	4.7550	8.9209
Case 2	11	2.7373	3.4717
Case 3	22	2.8490	4.8053

Table. 5 Error statistic for different sample size

4 LIMITATIONS AND FUTURE WORK

The current modelling is restricted to the attitude dynamics of a scaled helicopter. In future work, attitude parameters will be made functions of dynamic pressure and angle of attack, which is a common approach to modeling translational effects in the literature. Another addition will be including rotor RPM in the attitude parameters. For example, the method presented could be applied on various steady state RPM to get a number of altitude parameter values. These values can be correlated to RPM to bootstrap a more complex model.

Hence, the concept is to capture the complexity by interactions of simpler models rather than one very complex model that would be too computationally intense to utilise in real time. Note that when translational dynamics are included, the IMU will provide the translational velocities from integrating the accelerometers, so could be easily included in the model if required. A translational model will be needed to address guidance of the helicopter to known GPS coordinates and this extension will be investigated in the future as well.

In order to fully validate the present modelling approach, flight data from an aggressive execution of flight maneuvering is required, as was presented in [25]. Therefore further testing is required in a wider flight envelope to fully validate the effectiveness of the minimal modeling approach. However, the integral method has been shown to be very effective in quite complex models with relatively large number of parameters (e.g [13]). Hence further complexity could be added to the modeling as required to capture the measured data while still maintaining very fast and accurate system identification.

In addition, another validation of the modeling approach in this paper would be to use the disturbance profile identified from experiments to simulate the response of a proportional-derivative controller for a number of gains. The distribution of the error in the roll rate relative to a given reference could then be predicted and compared with flight tests. This general approach has been very effective in biomedical field [14], and the goal is to apply this approach in the rotorcraft UAV field.

5 CONCLUSION

A minimal modelling approach is presented, which simplifies a more complex model of a scaled helicopter, derived from first principles. Three methods of system identification were compared for identifying attitude dynamics. The methods are the integral method, EKF and non-linear regression. The integral method was ~30 times faster than EKF method and 15,667 times faster than non-linear regression. The integral method also had a similar accuracy to non-linear regression method.

For the EKF method, the state estimation process accounts for the system disturbances via the process noise matrix Q. With poor estimates of Q, the method was very sensitive to the initial states. With optimal values of Q, the system disturbances were compensated to produce estimates of the model parameters that gave a reasonable match with the measured data. However, the errors were nearly twice the errors of the integral method and non-linear regression method. The EKF method was also not suitable for identifying parameters over a time period less than 5s and requires time periods greater than 10s to satisfactorily converge. The integral method had none of these issues and combined with its fast computation has been demonstrated to be very suitable for this application.

The integral method was shown to be effective in identifying both coupled and decoupled models. Thus the method is very flexible and provides the capabilities of adding more complexity if required to capture measured response. The integral method has a further advantage that it can separate the disturbances explicitly from the intrinsic dynamics. The method presented was to identify the disturbances as a constant torque over a given time period with all the intrinsic

parameters fixed. The torque can be related to the equivalent actuator angle and thus has a convenient physical interpretation. This disturbance profile could be used for later control development.

ACKNOWLEDGEMENT

Rejina L.W. Choi acknowledges Stephan G. Schalk from Eindhoven University of Technology, Eindhoven, the Netherlands for his effort in program the Mobisense board for the data logging system on the helicopter.

REFERENCES

1. Morris, J.C., van Nieuwstadt, M., Bendotti, P.: Identification and control of a model helicopter in hover. In: American Control Conference, 1994, 29 June-1 July 1994 1994, pp. 1238-1242 vol.1232
2. Tischler, B.M.a.T.K.a.M.B.: System identification modeling of a model-scale helicopter. In. Journal of the American Helicopter Society, (2000)
3. Salman, S.A., Puttige, V.R., Anavatti, S.G.: Real-time validation and comparison of fuzzy identification and state-space identification for a UAV platform. In: Computer Aided Control System Design, 2006 IEEE International Conference on Control Applications, 2006 IEEE International Symposium on Intelligent Control, 2006 IEEE, 4-6 Oct. 2006 2006, pp. 2138-2143
4. Kallapur, A.G., Anavatti, S.G.: UAV Linear and Nonlinear Estimation Using Extended Kalman Filter. In: Computational Intelligence for Modelling, Control and Automation, 2006 and International Conference on Intelligent Agents, Web Technologies and Internet Commerce, International Conference on, Nov. 28 2006-Dec. 1 2006 2006, pp. 250-250
5. Lyashevskiy, S., Yaobin, C.: Nonlinear identification of aircraft. In: Control Applications, 1996., Proceedings of the 1996 IEEE International Conference on, 15-18 Sep 1996 1996, pp. 327-331
6. Kanade, M.L.C.a.a.W.C.M.a.T.: Modeling of Small-Scale Helicopters with Integrated First-Principles and System-Identification Techniques. In, Montreal, Canada 2002, pp. 2505-2516
7. Tischler, M.B., Remple, R.K.: Aircraft And Rotorcraft System Identification: Engineering Methods With Flight-test Examples. American Institute of Aeronautics and Astronautics, (2006)
8. Hyunchul Shim, D., Hyoun Jin, K., Sastry, S.: Control system design for rotorcraft-based unmanned aerial vehicles using time-domain system identification. In: Control Applications, 2000. Proceedings of the 2000 IEEE International Conference on, 2000 2000, pp. 808-813

9. Bruce P.D., S.J.E.F., and Kellett M.G.: maximum likelihood identification of a rotary-wing RPV simulation model from flight-test data. Paper presented at the Atmospheric Flight Mechanics Conference Boston, MA,
10. Raol, J.R., Girija, G., Singh, J., Engineers, I.o.E.: Modelling and parameter estimation of dynamic systems. Institution of Electrical Engineers, (2004)
11. Hanbo, Q., Guanqing, C., Hongxing, C., Yiping, Y.: A Grey-Modeling Research on a Small-Scale Autonomous Helicopter. In: Information Engineering and Computer Science, 2009. ICIECS 2009. International Conference on, 19-20 Dec. 2009 2009, pp. 1-4
12. C E Hann, M.S., A Rao, O Winn, N Wongvanich, X Chen: Minimal modelling approach to describe turbulent rocket roll dynamics in a vertical wind tunnel. Journal of Aerospace Engineering (2011).
13. Hann, C.E., Chase, J.G., Lin, J., Lotz, T., Doran, C.V., Shaw, G.M: Integral-based parameter identification for long-term dynamic verification of a glucose-insulin system model. Computer Methods and Programs in Biomedicine **77(3)**, 259-270 (2005).
14. Hann, C.E., Chase, J.G., Ypma, M.F., Elfring, J., Nor, N.M.H., Lawrence, P., Shaw, G.M.: The Impact of Parameter Identification Methods on Drug Therapy Control in an Intensive Care Unit. The Open Medical Informatics Journal **2**, 92-104 (2008).
15. Padfield, G.D.: Helicopter flight dynamics: the theory and application of flying qualities and simulation modelling. Blackwell Publishing, (2007)
16. Raptis, I.A., Valavanis, K.P., Moreno, W.A.: System Identification and Discrete Nonlinear Control of Miniature Helicopters Using Backstepping. J. Intell. Robotics Syst. **55**(2-3), 223-243 (2009). doi:10.1007/s10846-008-9295-5
17. Castillo, P., Lozano, R., Dzul, A.E.: Modelling and control of mini-flying machines. Springer, (2005)
18. Kim, S.K., Tilbury, D.M.: Mathematical Modeling and Experimental Identification of an Unmanned Helicopter Robot with Flybar Dynamics. Journal of robotic systems **21**(3), 95-116 (2004). doi:10.1002/rob.20002
19. Docherty, P.D., Chase, J.G., Lotz, T.F., Hann, C.E., Shaw, G.M., Berkeley, J.E., TeMorenga, L., Mann, J.I., McAuley, K.: Independent cohort cross-validation of the real-time DISTq estimation of insulin sensitivity. Comput. Methods Prog. Biomed. **102**(2), 94-104 (2011). doi:10.1016/j.cmpb.2010.08.002
20. Wong, X.W., Chase, J.G., Shaw, G.M., Hann, C.E., Lotz, T., Lin, J., Singh-Levett, I., Hollingsworth, L.J., Wong, O.S.W., Andreassen, S.: Model predictive glycaemic regulation in critical illness using insulin and nutrition input: A pilot study. Medical Engineering & Physics **28**(7), 665-681 (2006). doi:http://dx.doi.org/10.1016/j.medengphy.2005.10.015
21. Martini, A., Léonard, F., Abba, G.: Dynamic Modelling and Stability Analysis of Model-Scale Helicopters Under Wind Gust. Journal of Intelligent & Robotic Systems **54**(4), 647-686 (2009). doi:10.1007/s10846-008-9280-z
22. Chowdhary, G.a.L., Sven: Control of a VTOL UAV via Online Parameter Estimation. Paper presented at the AIAA Guidance, Navigation, and Control Conference and Exhibit, San Francisco, California, USA,
23. Abhijit G. Kallapur, S.S.A.a.S.G.A.: Application of Extended Kalman Filter Towards UAV Identification. In: Autonomous Robots and Agents. pp. 199-207. Springer, Berlin/Heidelberg (2007)

24. Ozbek, L.v.E., M: Online Estimation of the State and the Parameters in Compartmental Models Using Extended Kalman Filter. In: Trofimova, W.H.S.a.I. (ed.) Nonlinear Dynamics in the Life and Social Sciences. pp. 262-271. IOS Press, (2001)
25. V. Gavrilets, E.F., B. Mettler, M. Piedmonte and E. Feron: Aggressive Maneuvering of Small Autonomous Helicopters: A Human-Centered Approach. The International Journal of Robotics Research (2001).

APPENDIX

Notation

a	Main rotor lift slope
B	Tip loss factor
$c / c_2 / c_T$	Main/flybar/tail blade chord length
dL, dL_m	Differential lift elements for flybar and main rotor blade
R	Length of main rotor blade

R_1	Distance between rotor axis and flybar tip
R_2	Distance between rotor axis and flybar root
R_T	Length of tail rotor blade
$R_{IB,BF,IF}$	Rotation matrices between Inertial, Body, and Flybar frames
$R_{IB,BM,IM}$	Rotation matrices between Inertial, Body, and main rotor frames
L_T	Distance between tail rotor axis and c.g.
$L_1 ... L_9$	Linkage lengths in rotor hub assembly
n	Number of main/flybar/tail blades
l	Position along the main rotor blade
$c.g.$	Centre of gravity
I_{xx}	Rotation inertia about X_b axis
I_{yy}	Rotation inertia about Y_b axis
I_{zz}	Rotation inertia about Z_b axis
I_f	Flybar moments of inertial in flapping
K_g	Gyro gain for tail rotor
K_m	Motor reaction torque gain
M_ϕ	Moment about the X_b axis
M_θ	Moment about the Y_b axis
M_ψ	Moment about the Z_b axis
ρ	Air density
δ	Input cyclic command
I	Shortened notation of I_{xx}
ξ	Main blade orientation angle
β	Flybar flapping angle

Ω	Main rotor angular velocity
λ, λ_T	Inflow ratio for main rotor and tail rotor